ORIGINAL RESEARCH

The Institution of Engineering and Technology WILEY

Optimal coordination of electric vehicle charging and photovoltaic power curtailment in unbalanced low voltage networks: An experimental case

Andrés Felipe Cortés Borray[1,2] | Kalle Rauma[3,4] | Esther Torres[2]

[1]TECNALIA, Basque Research and Technology Alliance (BRTA), Derio, Spain

[2]Department of Electrical Engineering, University of the Basque Country (UPV/EHU), Bilbao, Spain

[3]Institute of Energy Systems, Energy Efficiency and Energy Economics, TU Dortmund University, Dortmund, Germany

[4]VTT Technical Research Centre of Finland, Espoo, Finland

Correspondence

Andrés Felipe Cortés Borray, TECNALIA, Basque Research and Technology Alliance (BRTA), Astondo Bidea, Building 700, Derio E-48160, Spain.
Email: andres.cortes@tecnalia.com

Abstract

This study introduces a quadratic programming-based optimisation method to coordinate electric vehicle (EV) charging and photovoltaic (PV) curtailment in unbalanced low voltage (LV) networks. The proposed model is defined as a convex model that guarantees the optimal global solution of the problem avoiding the complexity of non-linear models and surpassing the limitations of local solutions derived from meta-heuristics algorithms reported in the literature. The coordination is carried out through a centralised controller installed at the header of the LV feeder. The objective of the proposed strategy is to minimise the power curtailment of all PV systems and maximise the power delivered to all EVs by optimising at every time step a suitable setpoint for the PV units and the charging rate of each EV connected without surpassing network constraints. A new energy-boundary model is also proposed to meet the energy requirements of all EVs, which is based on a recurrent function that depends on the arrival-and-desired energy states of the vehicle to compute its charging trajectory optimally. The effectiveness of the proposed coordination strategy was successfully proven through three scenarios in a laboratory environment, making use of two commercial EVs and a PV inverter in a Power Hardware-in-the-Loop setup.

1 | INTRODUCTION

Nowadays, low voltage (LV) distribution networks face a fast growth of electric vehicles (EVs) and renewable energy sources such as solar photovoltaic (PV) due to cost reductions and subsequent demand. The evolution of this scenario has also been supported by a favourable policy context in terms of fiscal incentives, more strict emission standards, and support for charging infrastructure [1]. However, as shares of these technologies grow, the conventional distribution network requires adaptive measures to maintain or improve the energy service provision, for example, introducing control and monitoring systems to optimise the network capacity instead of network reinforcement.

In this context, different theoretical approaches to optimise EV charging and maximise PV power generation without exceeding the network capacity have been proposed in the literature. Fachrizal et al. [2] proposed a combined distributed charging scheme and PV curtailment for assessing the hosting capacity of LV networks. This strategy sought to minimise the net-load variability of a single household, that is, reducing both peak load and surplus generation. The study used a smart charging algorithm presented in Ref. [3]. The drawback of the algorithm is that it relies on a perfect forecast of the power consumption and PV production of a single home as well as on the knowledge of the state-of-charge (SOC) of the EV. Thus, any error in these estimations leads to non-optimal results.

In ref. [4], a charging coordination algorithm to utilise the grid-to-vehicle and vehicle-to-grid capabilities of EVs is proposed to minimise power losses, voltage profile deviation, and network unbalance. The algorithm intends to determine the proper phase for the EVs by operating the so-called "phase-switcher", a device in series with the charging station, which in turn both are linked to a central management centre. A

negative side of this algorithm is that it works only with single-phase EVs. It means that in real life, the system would not work with current three-phase EVs. Also, installing the phase-switcher increases the costs and adds a new point of failure to the system.

A smart charging strategy based on reactive power discharging and phase switching in unbalanced LV networks was proposed in ref. [5] to minimise the network losses and the charging cost of the users. The optimisation model was defined as a mixed-integer non-linear programming problem. Due to the non-convexity and non-linearity of the problem, a discrete particle swarm optimisation model was used to generate and update the control variables in combination with the direct load flow approach to evaluate the explored solutions. Nonetheless, using the meta-heuristic approach increases the complexity of the problem as it is treated like a non-linear non-convex optimisation problem that highly leads to getting stuck in a local solution. In a previous work [6], a coordination EV charging strategy based on a linear programmming model was defined. It aimed to maximise the EV's charging in an unbalanced grid by taking advantage of the PV power without exceeding the operational limits of the LV network, making use of its sensitivity coefficient matrices. However, this work did not consider managing the limitation of PV power injection into the network because the total installed PV capacity was lower than the nominal power value of the feeder. This means that the PV power was considered only as a parameter in network constraints instead of a variable.

Concerning PV power management to mitigate voltage limits violation problems in distribution networks, in ref. [7], a distributed control method to dispatch active and reactive power from the PV inverters is presented in order to minimise their operational costs, lead system voltage into an acceptable range and meet the network capacity constraints. This method was tested in a real-time simulator to validate its performance. Besides, the work in ref. [8] proposed a control approach to minimise the voltage unbalance, voltage deviation, active power losses and PV curtailment in the LV network as a multi-objective optimisation problem in combination with the Backward/Forward Sweep unbalanced three-phase power flow algorithm to drive a real-time energy management system in a network with batteries and a high share of PV. However, similar to ref. [5], the optimality of the problem highly depends on the parametrisation of the meta-heuristic algorithm and the complexity of the non-linear terms of the model, which implies that each solution, in this case, in the Pareto front may not be the optimal global value of the problem. Kontis et al. [9] presented a two-layer-based centralised approach to manage voltage regulation and voltage unbalances problems due to a high PV share in unbalanced low-voltage networks. The first control layer is embedded at the hardware level of the inverter to prevent overvoltages and voltage unbalances using local measurements. The second layer is located at the distribution system operator (DSO) level as a central controller to reallocate the PV curtailment. It is a fair-power-sharing algorithm in an on-load-tap-changer (OLTC) MV/LV transformer. Additionally, both authors in refs. [7, 9] employ a droop control to manage the PV curtailment based on local measurements. The former without considering the topology of the LV network using the Dual Gradient Descent algorithm to optimise the system power cost, and the latter, employing a deterministic approach based on multiple simulations using the polar form of the power flow equations to adjust the OLTC of the distribution transformer to meet the operational voltage of the LV network. In ref. [10], a coordinated reactive power compensation algorithm is proposed to mitigate overvoltages in the LV network with minimal PV power curtailment by using a battery energy storage system (BESS). It is based on the selection of a regulation node with the maximum voltage rise and the PV-BESS group with the highest voltage sensitivity to compute the required power curtailment. Battery systems are used to curtail surplus generation to prevent overvoltages and supply the lack of generation to prevent under-voltages. Both [9, 10] used the voltage sensitivity coefficients of the network to reallocate the PV curtailment among the PV units and find the PV compensation due to an overvoltage problem respectively. However, the voltage sensitivities were obtained assuming three-phase balanced LV networks. The former used the inverse Jacobian matrix and the latter from the partial derivatives of the cartesian form of the power flow equations.

On the other hand, there are other works that focus on the conceptual design of integrating PV systems with EV charging, such as [11–15]. All five studies, except [12], use additional energy storage to buffer the energy between the EVs and the PV units. In addition, the algorithms were tested through simulations, disregarding relevant real-world conditions, such as non-idealistic charging characteristics, so their performance is only approximate and may differ in real applications.

Experimental-based approaches are less encountered in the literature. For example, in refs. [16–18], a novel adaptive charging algorithm was developed. The algorithm is based on the actual charging current measurements instead of pre-defined load curves, which means that no modelling or data about the EVs is necessary. The algorithm is sought to maximise the charging current within the capacity limits of the network and reduce charging times. In general terms, the individual or combined analysis of EVs and PVs within a simulation framework are considered either as optimisation problems (e.g. linear [6], non-linear [2, 3, 7, 12] and meta-heuristic [5, 8]) or deterministic approaches [4, 9–11, 13–15]. However, to the knowledge of the authors, no paper considering a combined testbed for smart EV charging and PV curtailment is not found in the literature. Therefore, the aim of this work is to test in a laboratory environment a new coordination strategy to manage the EVs and PVs in unbalanced LV networks, considering the current limitations to implementing those approaches. This means convexify the power management problem in unbalanced LV networks when including network constraints to guarantee the optimal global solution of the model. Particularly, this paper uses the Perturb-and-Observe (P&O) approach to compute the voltage-and-loading sensitivity matrices of the unbalanced three-phase LV networks, which are included as a linearisation of network constraints in a quadratic programming (QP) model to

optimise the EV charging and power curtailment of al PV units. A new energy boundary model is defined to optimally compute the charging trajectory during the available connection time of the EVs. A weighting formulation is proposed to evenly distribute the power curtailment among all PV units in the network.

The rest of this paper is organised as follows. Section 2 describes the energy boundary model to optimise the EV charging trajectory. Section 3 presents the proposed optimisation model in the coordination strategy to manage the EVs and PVs in unbalanced LV networks. The description of the experimental setup used for testing the proposed optimisation model is presented in Section 4, and the experimental results are discussed in Section 5. The limitations of the proposed approach and future hints are discussed in Section 6. Finally, conclusions are drawn in Section 7.

2 | ENERGY BOUNDARIES OF EVS

This section introduces a new EV model based on the lower and upper power and energy boundaries of the battery in order to know how the charging trajectory evolves between these two energy states. This approach considers as main input parameters the EV arrival/departure time, the energy characteristics of the battery and the energy requirements of the users. The detailed battery model is described in ref. [6].

As the energy state previous to the EV connection is unknown, the arrival energy level e_j^{arr} is defined as the starting point for the upper and lower energy boundaries, as shown in Equation (1).

$$e_j^{\text{upper}}(t) = e_j^{\text{lower}}(t) = e_j^{\text{arr}} \quad \forall j \in N^{EV},$$
$$t = 0, \ldots, t_j^{arr} \tag{1}$$

Once the EV j is connected to the charging station, the upper energy boundary is recursively computed by Equation (2) within the interval of its arrival and the number of discrete time steps of the evaluation period N_{slots}. Note that the maximum energy state is the energy level defined by the user e_j^{obj}. Besides, the number of discrete-time slots N_{slots} is computed by considering a time step t_s and an interval length $\Delta t = t_s/(60 \text{ min})$ for a test period T, that is, $N_{\text{slots}} = T/\Delta t$.

$$e_j^{\text{upper}}\left(t_j^{\text{arr}} + t\right) = \min\Big\{e_j^{\text{upper}}\left(t_j^{\text{arr}} + t - 1\right)$$
$$+ p_{cb}^{\max} \cdot \eta_{cb} \cdot \Delta t, \ e_j^{\text{obj}}\Big\},$$
$$\forall j \in N^{EV}, \ t = 1, \ldots, N_{\text{slots}} - t_j^{\text{arr}} \tag{2}$$

On the other hand, the lower energy boundary of the EV j is also recursively calculated by Equation (3), setting e_j^{arr} as the minimum energy level of the battery. The way to obtain this boundary is equal to starting from a future state and going back to a past state.

$$e_j^{\text{lower}}\left(t_j^{\text{dis}} - t\right) = \max\Big\{e_j^{\text{lower}}\left(t_j^{\text{dis}} - t + 1\right)$$
$$- p_{cb}^{\max} \cdot \eta_{cb} \cdot \Delta t, \ e_j^{\text{arr}}\Big\},$$
$$\forall j \in N^{EV}, \ t = 1, \ldots, t_j^{\text{int}} + 1 \tag{3}$$

Equation (4) states that once the EV j is disconnected, its energy level must be equal to e_j^{obj} up to N_{slots}.

$$e_j^{\text{lower}}\left(t_j^{\text{dis}} + t\right) = e_j^{\text{obj}} \quad \forall j \in N^{EV},$$
$$t = t_j^{dis}, \ldots, N_{\text{slots}} - t_j^{\text{dis}} \tag{4}$$

Once the energy boundaries of all EVs are obtained, these are employed as constraints in the proposed optimisation problem.

3 | OPTIMISATION MODEL

When the number of PVs and EVs increases in the LV network without any control action, the voltage and loading levels of the grid can be negatively affected. Hence, to avoid that operational condition, the proposed optimisation problem seeks to minimise the power curtailment of all PV units and maximise the power delivered to all EVs by optimising at every time t a suitable setpoint for the PVs and the charging rate of each EV connected without surpassing network constraints. It is assumed that all households have installed smart metres with load and generation control capability. The optimisation process is carried out in a central controller at the head of the feeder in order to manage the PVs and EVs in a coordinated manner. In this sense, the optimisation problem is computed at each time t based on the (QP) model given by Equation (5).

$$\text{maximise } f_1 = \sum_{i \in H^{PV}} \left(\left(1 - \frac{p_{i,t}^{PV} \cdot \zeta_{i,t}}{p_{PV_i}^{\text{rated}}}\right) \cdot p_{i,t}^{PV} \cdot \zeta_{i,t}\right)$$
$$+ \sum_{i \in H^{EV}} \left(p_{i,t}^{EV} - \Delta_{i,t}^{P_{\text{inc}}}\right) \cdot x_{i,t} \tag{5}$$

Considering that all households with a PV unit can export the surplus energy to the grid, these units can also provide local voltage support through the active power curtailment set up for maintaining the voltage profile below a normative upper limit. In this case, at every time step, each PV inverter continuously checks the demand and its power output to adjust the generation setpoint through the factor $\zeta_{i,t}$. Note that the value of $\zeta_{i,t}$ highly depends on the voltage sensitivity coefficients of the network (constraint Equation (12)) to maintain the voltage within its operational limits. Hence, the first term in Equation (5) seeks to minimise the PV power curtailment of the ith household when an overvoltage or overload condition occurs. As all the PV units are likely to contribute to the aggregated reverse power flow, the PV power curtailed $\left(p_{i,t}^{PV} \cdot \zeta_{i,t}\right)$ is evenly distributed among all users by weighting.

The second term aims at maximising the charging power $\left(P_{i,t}^{EV}\right)$ of all EVs by dynamically adjusting the rate of power $\left(\Delta_{i,t}^{P_{inc}}\right)$ of their chargers, avoiding severe voltage drop conditions across the network caused by a high load level in the feeder. Note that H denotes the set of households supplied by the DSO, $p_{PV_i}^{\text{rated}}$ is the rated power of PV unit i, and $x_{i,t}$ is a binary matrix of $[H \times N_{\text{slots}}]$ such that $x_{i,t} = 1$ if the EV j is connected to the household i at time t, and $x_{i,t} = 0$ otherwise.

3.1 | The constraints of PVs and electric vehicles

For all PV units, constraint Equation (6) ensures that the total PV power per phase should not surpass the nominal capacity per phase of the main cable of the feeder $\left(p_{\text{Line}_{l,\phi}}^{\text{rated}}\right)$, where H_{ϕ}^{PV} is the number of households with a PV unit connected at phase ϕ.

$$\sum_{i \in H^{PV}} \left(p_{i,t}^{PV} \cdot \zeta_{i,t}\right) <= p_{\text{Line}_{l,\phi}}^{\text{rated}}, \forall l \in \text{Lines}, \ \forall \phi, \forall t \quad (6)$$

On the other hand, the charging rate of each EV is dynamically adjusted considering the energy level of its battery in order to avoid violating the technical limits of the grid as given in Equations (7)–(11). In this sense, Equation (7) sets that at any t, the charging power for the EV connected to the household i cannot surpass the charger rating power, where p_{ch}^{max} is the maximum charging power at the AC side of the charger, η_{ch} is the charger efficiency, and H^{EV} is the set of households with EV.

$$0 \le p_{i,t}^{EV} \le p_{ch}^{\text{max}} \cdot \eta_{ch}, \ \forall i \in H^{\text{EV}}, \forall t \quad (7)$$

Equation (8) seeks to limit sudden variations in the charging rate for consecutive time slots using a constant setpoint (Δ_P) in conjunction with a penalty deviation variable $\Delta_{i,t}^{P_{inc}}$, which relaxes the problem when necessary. This condition is defined for those EVs with narrow energy boundaries and that need a power boost in the next time step to not exceed their lower energy boundary.

$$p_{i,t-1}^{EV} - \left(\Delta_P + \Delta_{i,t}^{P_{inc}}\right) \le p_{i,t}^{EV} \le p_{i,t-1}^{EV} + \left(\Delta_P + \Delta_{i,t}^{P_{inc}}\right), \\ \forall i \in H^{\text{EV}}, \forall t \quad \text{if} \quad x_{i,t} \ne 0 \quad (8)$$

Equation (9) guarantees that any increase in the charging rate of the EV at household i should be no greater than the left capacity of the charger, that is, $\Delta_{\text{max}}^{P} = p_{ch}^{\text{max}} \cdot \eta_{ch} - \Delta_P$.

$$0 \le \Delta_{i,t}^{P_{inc}} \le \Delta_{\text{max}}^{P}, \ \forall i \in H^{\text{EV}}, \forall t \quad (9)$$

Finally, Equation (10) states that at every time t, the energy level of the jth vehicle connected to household i must be within the energy boundaries computed in Section 2. The computation of the current energy state is given by Equation (11), which considers the arrival time of vehicle j $\left(t_j^{arr}\right)$, the charging power at time t, and the energy level from the previous period $\left(t_j^{arr} + t - 1\right)$.

$$e_i^{\text{lower}}\left(t_j^{arr} + t\right) \le e_i^{EV}\left(t_j^{arr} + t\right) \le e_i^{\text{upper}}\left(t_j^{arr} + t\right), \\ \forall i \in H^{\text{EV}}, \forall j \in N_{EV}, t = 0, \ldots, t_j^{int} + 1 \quad (10)$$

$$e_i^{EV}\left(t_j^{arr} + t\right) = \begin{cases} e_j^{arr} + p_i^{EV}\left(t_j^{arr} + t\right) \cdot \Delta t, & t = 0, \ \forall i \in H^{\text{EV}}, \forall j \in N^{EV} \\ e_i^{EV}\left(t_j^{arr} + t - 1\right) + p_i^{EV}\left(t_j^{arr} + t\right) \cdot \Delta t, & t = 1, \ldots, t_j^{int} + 1, \end{cases} \quad \forall i \in H^{\text{EV}}, \forall j \in N^{EV} \quad (11)$$

3.2 | Network constraints

In order to evaluate the effect of the voltage and loading level of the feeder in the coordination strategy, the linear approximations for these two parameters in ref. [6] were modified to include the PV power curtailment factor $\zeta_{i,t}$. As these approximations depend on the voltage-and-loading sensitivity coefficients of the network, these matrices are obtained using the P&O method described in ref. [6]. This performs several unbalanced three-phase load flow in steady-state through PowerFactory [19] in conjunction with Python [20]. In this sense, Equation (12) ensures that voltage magnitude is within the operating limits given by the DSO when significant voltage variations occur due to new connections of EVs and PVs in the LV network.

$$V_{\text{min}} \le V_{i,t}^{\text{fc}} + \mathbf{A}_{i,i} \cdot p_{i,t}^{EV} + \mathbf{B}_{i,i} \cdot p_{i,t}^{PV} \cdot \zeta_{i,t} \\ + \sum_{\substack{h \in H \\ i \ne h}} \left(\mathbf{A}_{h,i} \cdot p_{h,t}^{\text{EV}} + \mathbf{B}_{h,i} \cdot p_{h,t}^{PV} \cdot \zeta_{h,t}\right) \le V_{\text{max}}, \\ \forall i \in H^{\text{EV}}, \forall t \quad (12)$$

where $V_{i,t}^{fc}$ is the forecasted voltage at load node i; $\mathbf{A}$ and $\mathbf{B}$ are two square matrices of $[H \times H]$ that represent the voltage sensitivity coefficients by the connection of new loads and generation respectively. This means that voltage sensitivity in $\mathbf{A}$ quantifies the voltage drop by increasing demand in a load node, whereas, in $\mathbf{B}$, this sensitivity value will be positive to represent the voltage rise by injecting power. Besides, $V_{\min}$ and $V_{\max}$ define the minimum and maximum network voltage levels defined by the DSO. The term $i \neq h$ means that i remains fixed while h varies.

To not exceed the operational limits of cables and transformers in the LV network, the active power flow derived from the PV generation, and EV demand must be optimally controlled. This task is carried out by Equations (13) and (14).

$$P_{\text{Line}_{l,\phi,t}}^{fc} + \sum_{\substack{b \in H \\ b \neq \varnothing}} \left(\mathbf{C}_{b,\phi,l} \cdot p_{b,t}^{EV} + \mathbf{D}_{b,\phi,l} \cdot p_{b,t}^{PV} \right)$$

$$\leq S_{\text{Line}_{l,\phi}}^{\text{rated}} \cdot \cos(\varphi), \quad \forall l \in \text{Lines}, \forall \phi, \forall t \in N_{slots} \quad (13)$$

$$P_{\text{Trans}_{k,\phi,t}}^{fc} + \sum_{\substack{b \in H \\ b \neq \varnothing}} \left(\mathbf{F}_{b,\phi,k} \cdot p_{b,t}^{EV} + \mathbf{G}_{b,\phi,k} \cdot p_{b,t}^{PV} \right)$$

$$\leq S_{\text{Trans}_{k,\phi}}^{\text{rated}} \cdot \cos(\varphi), \quad \forall k \in \text{Trans}, \forall \phi, \forall t \in N_{slots} \quad (14)$$

where $P_{\text{Line}_{l,\phi,t}}^{fc}$ and $P_{\text{Trans}_{k,\phi,t}}^{fc}$ are the forecasted loading levels per phase ϕ of the main cable l and distribution transformer k at time t. These two parameters can be obtained through the unbalanced quasi-dynamic power flow for the whole test period T considering a demand forecasting scenario for the network. $\mathbf{C}$, $\mathbf{D}$, and $\mathbf{F}$, $\mathbf{G}$ are three-dimensional matrices of $[H \times \phi \times \text{Line}]$ and $[H \times \phi \times \text{Trans}]$ that represent the loading sensitivity coefficients per phase of the service cable l and distribution transformer k. A positive sensitivity value in $\mathbf{C}$ and $\mathbf{F}$ represents an increase of the loading level on the main cable, whereas, in $\mathbf{D}$ and $\mathbf{G}$, those values are negative, indicating a reduction in the loading level. Only one set of sensitivities is calculated along the test period, as this approach reduces the computational burden and execution time of the algorithm. $S_{\text{Line}_{l,\phi}}^{\text{rated}} \cdot \cos(\varphi)$ and $S_{\text{Trans}_{k,\phi}}^{rated} \cdot \cos(\varphi)$ illustrate the rated active power per phase for both the service cable l and the distribution transformer k. The term $h \neq \varnothing$ means that those households without a PV or an EV unit are skipped.

4 | DESCRIPTION OF THE EXPERIMENTAL SETUP

In order to verify the real performance of the proposed co-ordination strategy described in Section 3, an experimental test case was carried out at the Smart Grid Technology Lab at TU Dortmund University, Germany. As illustrated in Figure 1, the laboratory is equipped with different assets such as LV cables emulators, on-load tap changer transformers, redox-flow batteries, power amplifiers, hardware for real-time simulations, controllable loads, a PV inverter, EVs and EV charging stations. A complete description of the laboratory can be found in ref. [21].

The proposed coordination strategy was implemented in Python and tested by using the infrastructure for EV charging and PV control (see Figure 1), which is described as follows. An RWE eSTATION charging station with a Phoenix Contact Advanced EV charging controller [22]. This charging controller allows limiting the current up to 32 A and receiving the setpoints of current via Modbus TCP/IP protocol. The charging station is equipped with two independent charging outlets up to 11 kW (400 V AC). In order to represent the smart metre from a real case, a KoCoS EPPE CX power quality analyser was installed in one of the charging outlets to measure the voltage, current, and active power from the grid.

Taking into account the technical characteristics of the charging station, two commercial EVs with charging currents between 6 and 16 A were tested: a Nissan Leaf with a single-phase connection up to 3.7 kW (16 A/230 V AC) and a BMW i3 with a three-phase connection up to 11 kW (16 A). The technical characteristics of the tested EVs are presented in Table 1.

Besides, a 60 kVA SMA inverter [23] and a 200 kVA EGSTON [24] power amplifiers group (see Figure 1) were used in a Power Hardware-in-the-Loop (PHiL) setup, as shown in Figure 2, in conjunction with Python to send the optimal power curtailment signal to the PV inverter. A supervisory control and data acquisition interface controls both power amplifiers. In this setup, the PV power at the DC side of the inverter is provided by one of the power amplifiers (configured in DC bipolar current mode) by a single cell PV model developed in RT-Lab [25]. The PV inverter is connected along with a variable resistive load to the busbar 2 (the cabinet in the middle). The variable load was not used in this setup. The other power amplifier is employed to emulate the AC three-phase-four-wire source connected to the same busbar.

On the other hand, a distribution feeder from one real LV network in the North West of England [26] was modelled in PowerFactory to allocate a set of EVs and PV systems. Ten households with EVs and PV units were considered, assuming that all vehicles arrive at 11:00 h in order to take advantage of the available PV power. A time resolution of 1 min was considered to be accurate for this study [27].

Figure 3 shows a simplified schema of the employed setup. The yellow block represents the central controller at the analysed feeder. Here, the coordination strategy described in Section 3 is computed at each time t. Before starting the connection with the charging station and the PV inverter, that is, at $t - 1$, the sensitivity coefficients of the network are computed in PowerFactory. Then, from $t = 0$ to the time when the simulated PV power is greater than zero, the optimisation runs in simulation time, that is, in a few seconds. Afterwards, the connection with the PV inverter is established using the
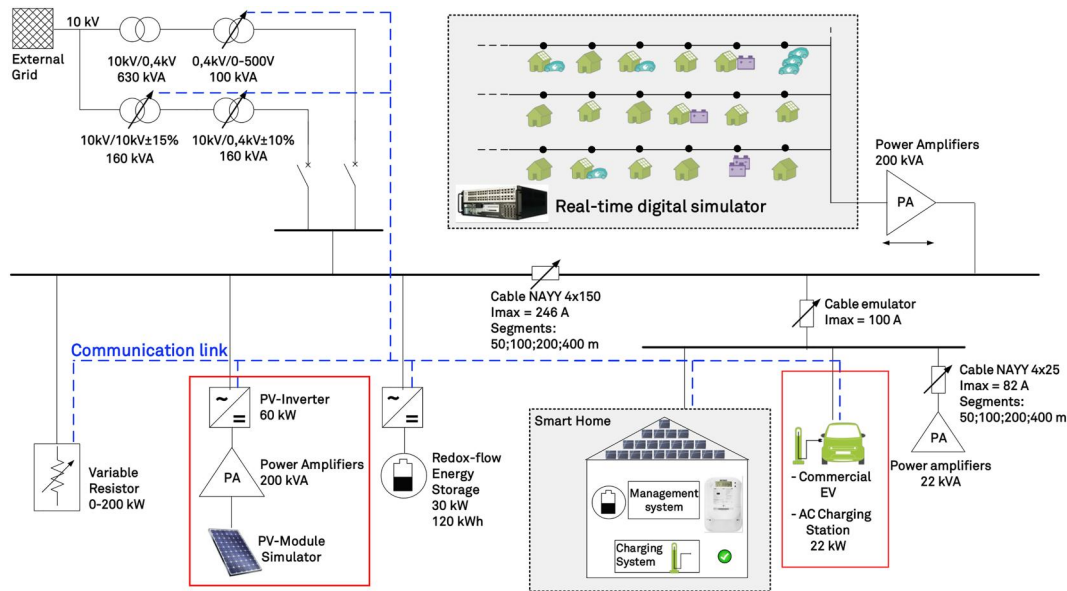
FIGURE 1 Smart Grid Technology Lab layout. Adapted from [21].

TABLE 1 Technical characteristics of the tested vehicles

Vehicle	Nissan Leaf 2012	BMW i3 2016
Battery capacity	24.1 kWh	33.2 kWh
On-board charger efficiency	0.89	0.93
Connector IEC 62196	Type 1	Type 2
Max. Charging current	16 A	16 A
AC topology	1-phase	3-phase

FIGURE 2 Experimental setup for the photovoltaic (PV) inverter operation.

Modbus library (ModbusTcpClient) in Python to read the active power and send the optimal power curtailment signal when required. This process is carried out every 1 min. Note that the connection with the charging station and the power analyser can be established before or after the connection with the PV inverter. This is given by the arrival time of the emulated vehicles. Once set the connection, every 1 min, the optimal current setpoint is sent to the charging controller, and the voltage, current and active power are read at the charging point. This process is repeated until the EVs emulated are disconnected. For the PV unit, its disconnection occurs in the later afternoon when no solar radiation is available. Once the device with the greatest disconnection time is not already available, either the PV inverter or the charging station, the optimisation runs again in simulation time up to the end of the test period.

Due to the limitation of measuring one charging outlet, two scenarios were tested. One scenario with one PV unit emulated and nine PV units simulated, nine EVs simulated and one EV emulated (the green star in Figure 3 depicts both the Nissan Leaf and the SMA inverter), and another scenario with all 10 PV units simulated, seven EVs simulated, and three EVs emulated. The red stars in Figure 3 represent the BMW i3. The three-phase AC topology of the BMW i3 and its capability to control each phase individually allowed emulating the performance of three EVs. Besides, it was assumed that all PV units have a rated power of 5 kVA operated with a unity power factor.

Since it is not possible to get access to the SOC of both EVs when these are connected to the charging station, it was necessary to perform the following procedure before the experimental test. First, the EVs were fully charged to be driven on a round-trip of approximately 23.4 km (see Figure 4) from the Smart Grid Technology Lab. Then, the vehicles were connected again to the charging station to measure the left energy needed to be fully charged. During this test, it was found that the energy necessary to reach the rated battery capacity of the Nissan Leaf and the BMW i3 was 3.8 and
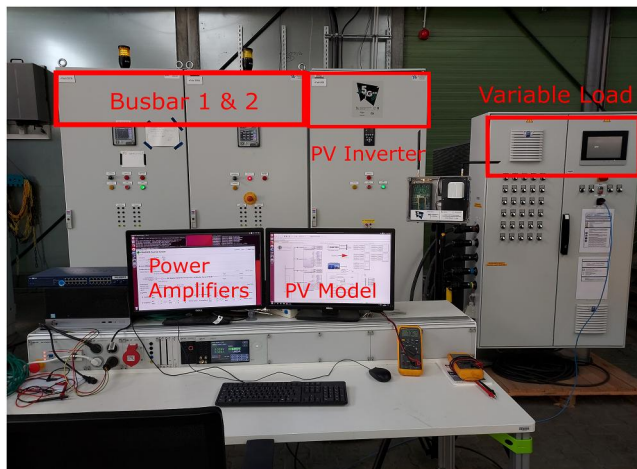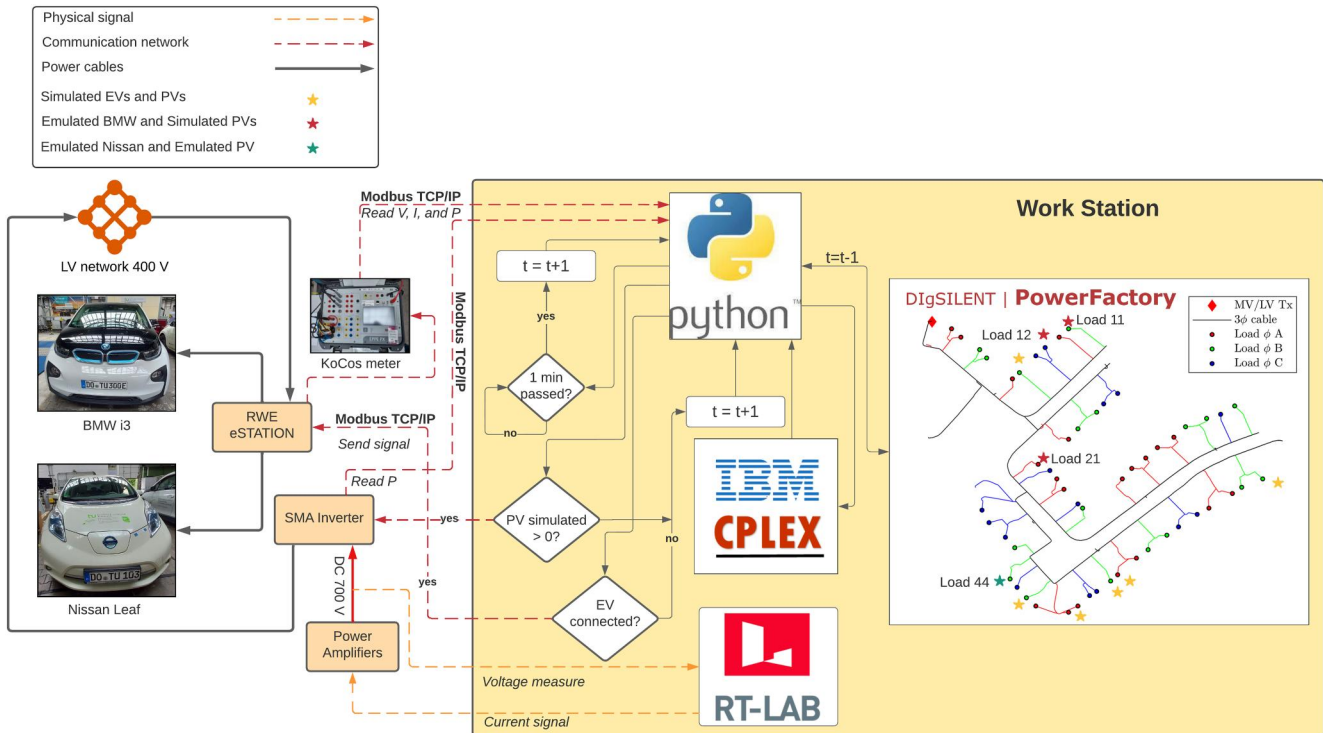
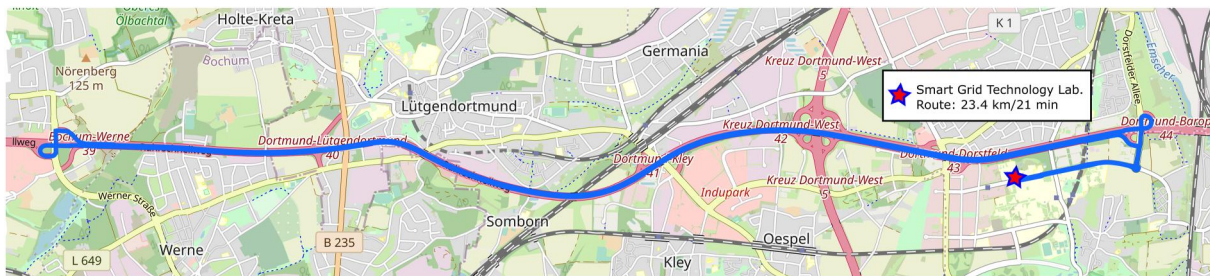**FIGURE 3** Simplified scheme of the laboratory setting.

FIGURE 4 Testing route for the Nissan Leaf and BMW i3.

2.9 kWh respectively. Note that these values can vary for the same route because they highly depend on the driving mode, state of the tyres, average velocity, and other external factors that can modify the energy consumption rate (kWh/km) of the vehicles.

Afterwards, the same route was driven again, trying to keep the initial drive mode to carry out the experimental test in Figure 3. Then, with the above-found energy values, the arrival energy of both EVs was estimated by subtracting them from the nominal battery capacity of each vehicle.

5 | EXPERIMENTAL RESULTS

This section presents the results obtained by employing the proposed coordination strategy under the experimental case described above.

5.1 | First scenario results

In this scenario, Figures 5 and 6 compare the simulated and measured charging power/energy for the Nissan Leaf. It can be seen in both figures that the EV starts charging 1 min after being connected with a $\Delta_P = 1.38$ kW, that is, 6 A, which is the minimum current to activate the charging controller. Thereafter, the charging power continues increasing up to the maximum charging power, that is, 3.7 kW. It can also be noticed that the measured power follows the optimal charging set point with small deviations associated with the instant where the measure was taken (a zoom view in Figure 6). In Figure 6 it is observed that the Nissan Leaf reached the nominal battery capacity value at the interval 730 (12:10 h) due to the charging process followed the upper energy boundary, which left an availability interval of 40 min (blue line in Figure 5).

Considering the size of the SMA inverter and that all PV units have a 5 kVA capacity, a scale factor of 10 was applied to the optimal value of the PV unit emulated in order to obtain a better response in the output power of the real inverter, that is, if the optimal setpoint was 2.5 kW, the inverter operated at 25 kW.

As a result of this approach, Figure 7 compares three PV power profiles: one profile obtained without any control on the PV inverter and the simulated and measured PV power profile considering the power curtailment factor ζ. It can be noted that the simulated PV power curves are based on a clear day close to ideal test conditions. However, the output power of the real inverter presents fast variations due to its maximum power point tracker algorithm, particularly for low power values.

5.2 | Second scenario results

For this scenario, Figures 8 and 9 compare the simulated and measured charging power/energy of the EVs connected at

households 11, 12, and 21, which are represented by the three-phase connection of the BMW i3. These users were selected because these are connected to the phases c, b, and a respectively. For the three vehicles, the charging process is delayed 2 min after being connected. Like the above scenario, the initial charging power equals 1.38 kW and continues to increase up to 3.7 kW. In this case, the measured power tries to follow the optimal set point, but it keeps below the reference for EVs in households 12 and 21. According to the charging tests carried out in the same laboratory by Caro et al. [28], this happens because the on-board charger injects unbalanced charging currents, that is, the current through phase a is greater than in phase b, and the current in phase b is higher than in phase c. Due to the constant voltage stage from the constant current-constant voltage (CCCV) algorithm in the DC-DC converter

FIGURE 5 Simulated and measured optimal charging profile for the electric vehicle (EV) located at household 44.

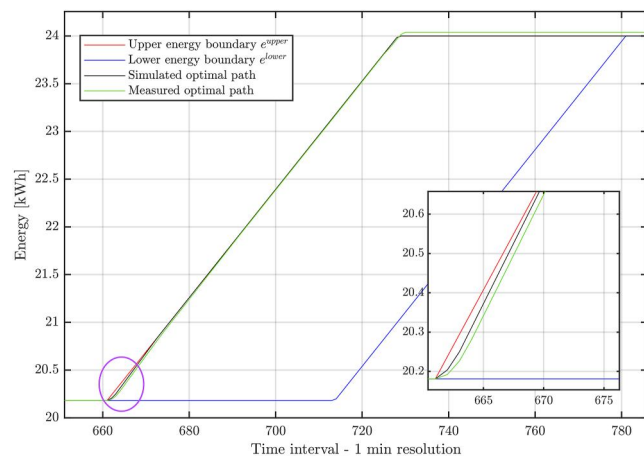**FIGURE 6** Simulated and measured optimal energy trajectories for the electric vehicle (EV) located at household 44.
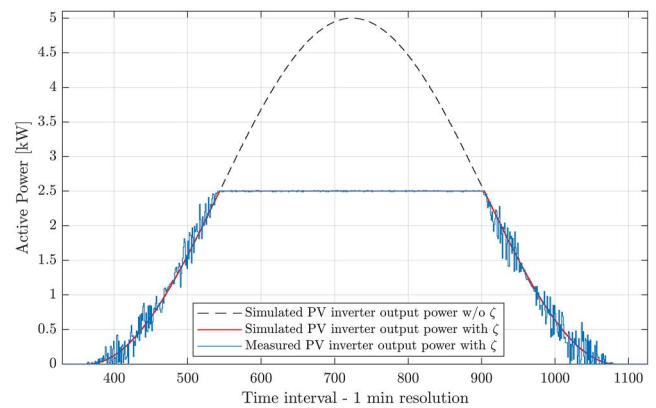

FIGURE 7 Comparison of the simulated and measured photovoltaic (PV) inverter output power at household 44 considering the optimal power curtailment factor ζ.
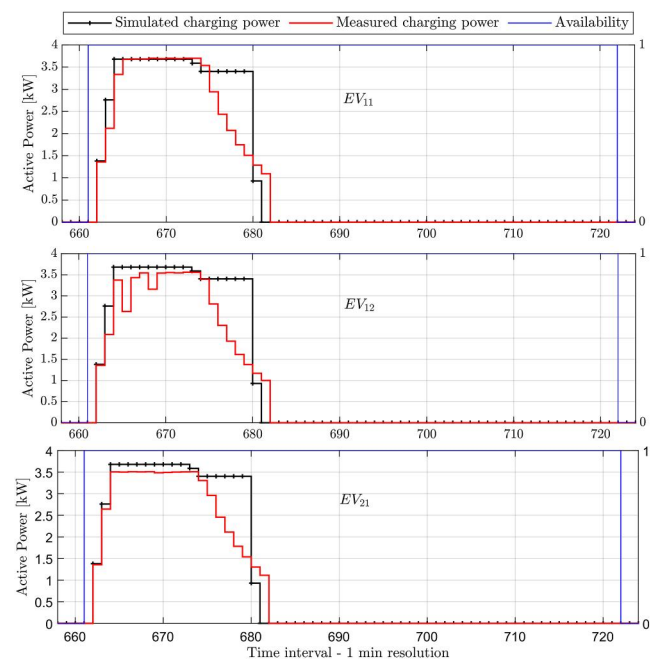

FIGURE 8 Simulated and measured optimal charging profile for the electric vehicles (EVs) located at households 11, 12, and 21.

of the BMW i3, the charging current starts to decrease even when the setpoint sent to the charging station is higher. This is because the traction battery reaches its maximum *SOC*.

Due to the difference between the optimal charging power and the measured power, an energy variation (Δ_E) exists at the end of the charging period, as shown in Figure 9. It is also noted that the nominal energy value of all three vehicles is
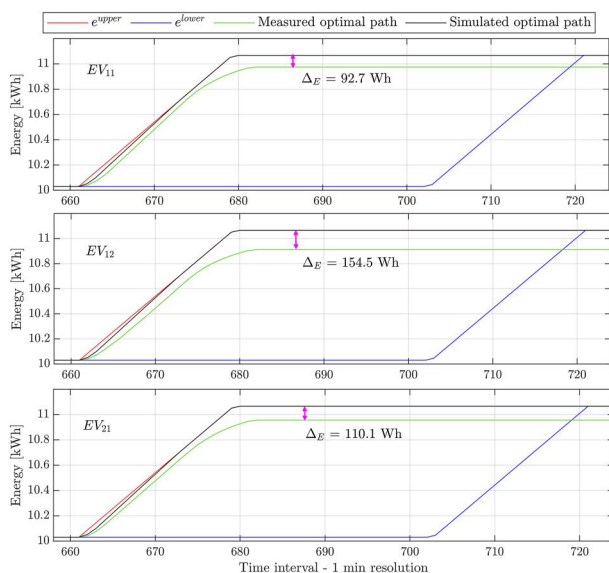

FIGURE 9 Simulated and measured optimal energy trajectories for the electric vehicles (EVs) located at households 11, 12, and 21.

reached before their maximum disconnection time because the charging process followed the upper energy boundary.

5.2.1 | Long-distance trip case

With the aim of testing the coordination strategy considering a lower SOC in the BMW i3, a round trip of approximately 132 km was performed (see Figure 10), starting with the vehicle fully charged from the Smart Grid Technology Lab to the Düsseldorf centre. At the arrival, the energy level of the vehicle was approximately equal to 13.2 kWh (4.38 kWh per emulated vehicle), which was estimated through $e_j^{arr} = e_j^{Bmax} - ECR_j \cdot d_j$, knowing the travelled distance d, the battery capacity and an $ECR = 0.153$ kWh/km from the interface of the vehicle.

The new test was configured and executed as in the second scenario, but this time with a lower arrival energy state. The results of the simulated and measured charging power/energy of the EVs connected at households 11, 12, and 21 are depicted in Figures 11 and 12. In Figure 11, the measured charging power in the emulated EVs closely follows the optimal charging setpoint before the interval 763 (12:43 h), when the CCCV algorithm in the BMW i3 automatically starts to decrease the value of the charging power in all three vehicles, that is, in the three phases. However, when the charging process is almost finished, a peak power value of 2.3 kW appears in phase *a* at interval 772 (12:52 h), which slowly decreases for approximately 8 min up to the
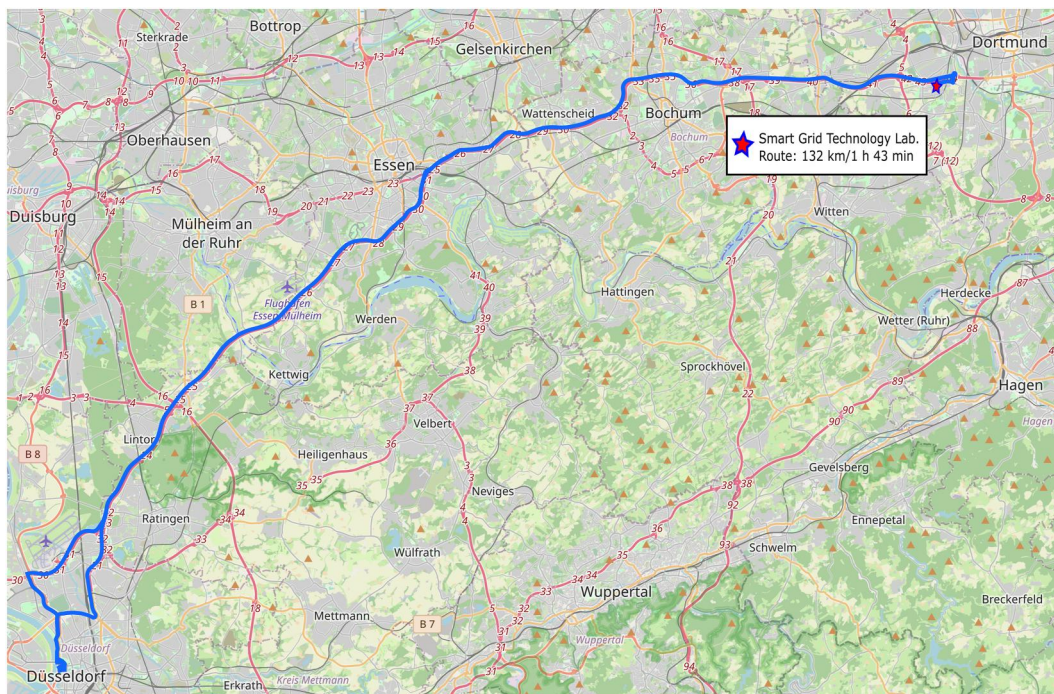

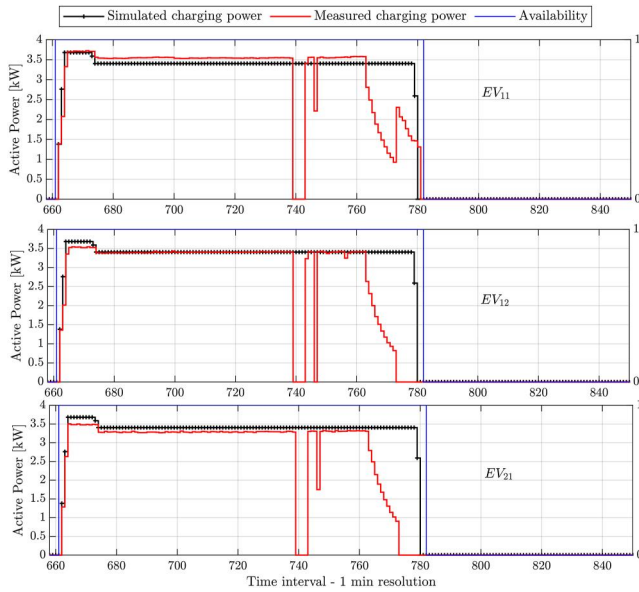**FIGURE 10** Testing route for a long trip with the BMW i3.

FIGURE 11 Simulated and measured optimal charging profile for the electric vehicles (EVs) located at households 11, 12 and 21 after performing a long trip.
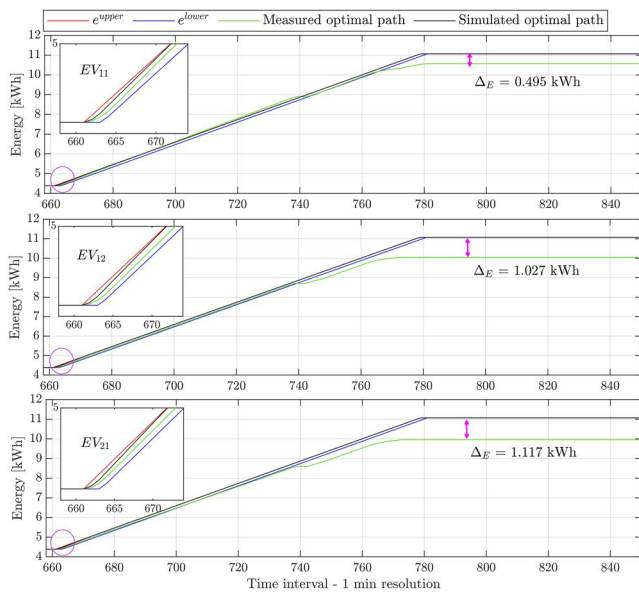

FIGURE 12 Simulated and measured optimal energy trajectories for the electric vehicles (EVs) located at households 11, 12, and 21 after performing a long trip.

disconnection time. Caro et al. [28] suggested that the reason why the charging power increases in phase a at the end of the charging period is because it is likely to be connected to a single-phase converter that supplies power to an auxiliary battery of the vehicle for all the visual indicators and the charging control of the BMW i3.

In terms of energy, Figure 12 shows that the optimal and measured charging energy paths in all three EVs follow a similar trajectory within their energy boundaries at the beginning of the charging process. However, the measured energy is kept constant for about 3 min from interval 739 (12:19 h) because the charging station was intentionally disconnected (Figure 11) in order to test the recovery of the charging process in all three phases. By doing so, the measured energy path of all phases deviates from the computed trajectory, deriving in a higher Δ_E at the end of the charging process, especially for phases b and c. This effect is due to the lack of feedback signals in the proposed coordination strategy, that is, it is not possible to execute a correction action under these perturbations in the optimisation. Besides, by comparing Figures 9 and 12, it can be observed that the longer the available range of EV connection, the narrower its energy boundaries, and therefore, the maximum time of delaying to start charging. When the battery energy level is over almost 95% (i.e., ≈10.5 kWh per emulated vehicle), no matter the control signal sent to the external charging controller, the internal CCCV algorithm dictates the charging power, as shown in both scenarios. Therefore, this is a limitation that cannot be controlled as it depends on the manufacturer, and therefore, the energy level that can be guaranteed is that in which the external control signal dictates the charging power.

6 | LIMITATIONS AND FUTURE WORK

Some limitations of the proposed approach are related to the utilisation of a unique set of sensitivity matrices for the whole optimisation period and that only the loading level of the main service cable of the feeder is evaluated. For the former, it means that the sensitivity values cannot be expected to exactly match those that could be computed for the load and generation levels at time $t + 1$ on the feeder, and for the latter means that if there is an overload condition in any of the branches, it cannot be evaluated; although these can be included in the construction of the sensitivity matrix. Another consideration for the sensitivity coefficients is the effect of network re-configuration, as the changes in feeder admittance will modify the sensitivity values of the grid. However, at the LV level, the number of possible re-configurations is almost null, and these operational states do not occur frequently.

On the other hand, the convexity assumption causes some limitations in terms of applicability, that is, the proposed approach requires a convex formulation of the optimisation problem because, without convexity, this model is not guaranteed to converge. Convexity allows for theoretical guarantees that the proposed quadratic optimisation model converges to the optimal solution. This leads to simplifying models by not including certain constraints or do not fully assure the control requirements. For example, tread network constraints as an optimal power flow problem by linearising the power flow

equations or, as in this case, considering the sensitivity coefficients of the network.

Future studies on the proposed approach are focussed on including the network restrictions either as a complex approximation or a second-order cone model in order to extend the coordination strategy to the utilisation of local battery energy storage systems to manage the surplus power from the PV units. Another direction is to include a receding horizon closed-loop control to deal with uncertainties linked to the base demand of the users, sudden departure times, and PV availability.

7 | CONCLUSION

A new coordination strategy to maximise the EV charging and minimise the PV curtailment in real LV networks was presented and tested in a laboratory environment to demonstrate its effectiveness in maintaining or improving the energy service provision by the DSO. The coordination strategy was defined as a quadratic optimisation model subject to a series of constraints related to the electrical characteristics of EVs and PVs, as well as the distribution network.

Experimental studies proved the concept of the coordination schema in Figure 3 by comparing the charging process of two commercial EVs and the power curtailment of a real PV unit. For the EVs, slight variations in power with respect to the optimal power value were found for the first vehicle, whereas for the second vehicle, these variations were more significant due to the internal charging control algorithm of the EV. Although the output power of the PV inverter varied significantly due to its size, the power curtailment factor was successfully applied based on the optimisation results. To achieve the above response by the PV inverter, it must be capable of limiting the active power through external signals.

In order to fully extend advanced smart charging strategies to real applications, it is necessary to account for a communication infrastructure that avoids wired installations to cover long distances (as is required by implementing Ethernet technology), for example, using the 5G network. Besides, the EV manufacturers should enable the option to access the vehicle parameters such as SOC, travelled distance, and time of charging in order to better quantify the energy requirements of the users.

AUTHOR CONTRIBUTIONS

Andres Felipe Cortés Borray: Conceptualisation, Formal analysis, Funding acquisition, Investigation, Methodology, Software, Validation, Visualisation, Writing – original draft, Writing – review & editing. **Kalle Rauma:** Conceptualisation, Methodology, Resources, Software, Supervision, Validation, Writing – review & editing. **Esther Torres:** Conceptualisation, Supervision, Writing – review & editing.

ACKNOWLEDGEMENTS

NOMENCLATURE

SETS

Lines	number of main distribution lines
Trans	number of distribution transformers
ϕ	number of phases
H	number of households of the network
H^{EV}	households with an EV
H^{PV}	households with a PV unit

PARAMETERS

Δ^P_{max}	remaining capacity of the charger in kW
$\cos(\varphi)$	load power factor in p.u.
Δ_P	fixed rate of charge in kW
η_{ch}	charging efficiency in p.u.
A	voltage sensitivity matrix for load changes in V/kW
B	voltage sensitivity matrix for generation changes in V/kW
C	loading sensitivity matrix for load changes in kW/kW
D	loading sensitivity matrix for generation changes in kW/kW
F	loading sensitivity matrix for load changes in kW/kW
G	loading sensitivity matrix for generation changes in kW/kW
d_j	travelled distance of EV j in km
e^{obj}_j	energy level defined by the user of EV j
$e^{B\max}_j$	maximum battery capacity of EV j in kWh
ECR_j	energy consumption rate of EV j in kWh/km
$P^{fc}_{\text{Line}_{l,\phi,t}}$	forecasted loading level per phase ϕ of feeder line l in kW
$P^{fc}_{\text{Trans}_{k,\phi,t}}$	forecasted loading level per phase ϕ of transformer k in kW
p^{rated}_{AC}	AC rated power of PV unit i in kW
$p^{\max}_{ch}$	maximum charging power from the grid side in kW
$p^{PV}_{i,t}$	active power of PV unit i at time t in kW
$S^{\text{rated}}_{\text{Line}_{l,\phi}}$	rated capacity per phase ϕ of the feeder main cable l in kVA
$S^{\text{rated}}_{\text{Trans}_{k,\phi}}$	rated capacity per phase ϕ of the distribution transformer k in kVA
T	test period in h
t_s	time step in min
t^{arr}_j	arrival time at home for the EV j

t_j^{dis}	disconnection time for an EV j
t_j^{int}	discrete-time intervals for an EV j parked at home
$V_{\max}$	maximum operating voltage limit in V
$V_{\min}$	minimum operating voltage limit in V
$x_{i,t}$	availability of EV in the household i at time t

VARIABLES

Δt	interval length
Δ_E	energy variation at the of the charging period in Wh or kWh
$\Delta_{i,t}^{P_{inc}}$	penalisation variable for dynamically adjusting the rate of charge of the EV connected to household i at time t in kW
$\zeta_{i,t}$	continuous variable for the power curtailment of PV unit connected to household i at time t in p.u.
e_i^{EV}	energy state of the EV connected at household i in kWh
$e_j^{\text{lower}}(t)$	lower energy boundary of EV j in kWh
$e_j^{\text{upper}}(t)$	upper energy boundary of EV j in kWh
e_j^{arr}	arrival energy level of EV j in kWh
N_{slots}	number of discrete time slots
$p_{i,t}^{EV}$	continuous variable for the charging power of the EV connected to household i at time t in kW

CONFLICT OF INTEREST

The author declares that there is no conflict of interest that could be perceived as prejudicing the impartiality of the research reported.

DATA AVAILABILITY STATEMENT

The data that support the findings of this study are available from the corresponding author upon reasonable request.

ORCID

Andrés Felipe Cortés Borray https://orcid.org/0000-0002-7819-2458

REFERENCES

1. REN21.: Renewables 2021 Global Status Report, Paris (2021). https://www.ren21.net/gsr-2021/
2. Fachrizal, R., et al.: Combined PV–EV hosting capacity assessment for a residential LV distribution grid with smart EV charging and PV curtailment. Sustain. Energy, Grids Netw. 26 (2021). https://doi.org/10.1016/j.segan.2021.100445
3. Fachrizal, R., Munkhammar, J.: Improved photovoltaic self-consumption in residential buildings with distributed and centralized smart charging of electric vehicles. Energies. 13(5), 1153 (2020). https://doi.org/10.3390/en13051153
4. Kikhavani, M.R., Hajizadeh, A., Shahirinia, A.: Charging coordination and load balancing of plug-in electric vehicles in unbalanced low-voltage distribution systems. IET Gener., Transm. Distrib. 14(3), 389–399 (2020). https://doi.org/10.1049/iet-gtd.2019.0397
5. Fu, Y., et al.: Coordinated optimisation of PEV charging with the support of reactive discharging and phase switching in unbalanced active distribution networks. IET Gener., Transm. Distrib. 14(21), 4703–4710 (2020). https://doi.org/10.1049/iet-gtd.2020.0117
6. Cortés Borray, A.F., et al.: New energy bound-based model for optimal charging of electric vehicles with solar photovoltaic considering low-voltage network's constraints. Int. J. Electr. Power Energy Syst. 129(January), 106862 (2021). https://doi.org/10.1016/j.ijepes.2021.106862
7. Kang, W., et al.: Distributed real-time power management of high-penetrated PV sources with voltage regulation over time-varying networks. Int. J. Electr. Power Energy Syst. 216, 129 (2021). https://doi.org/10.1016/j.energy.2020.119069
8. Camilo, F.M., et al.: Energy management in unbalanced low voltage distribution networks with microgeneration and storage by using a multi-objective optimization algorithm. J. Energy Storage. 33, 102100 (2021). https://doi.org/10.1016/j.est.2020.102100
9. Kontis, E.O., et al.: A two-layer control strategy for voltage regulation of active unbalanced LV distribution networks. Int. J. Electr. Power Energy Syst. 111, 216–230 (2019). https://doi.org/10.1016/j.ijepes.2019.04.020
10. Zhang, Z., et al.: High-economic PV power compensation algorithm to mitigate voltage rise with minimal curtailment. Int. J. Electr. Power Energy Syst. 125, 106401 (2021). https://doi.org/10.1016/j.ijepes.2020.106401
11. Li, S., et al.: Performance investigation of a grid-connected system integrated photovoltaic, battery storage and electric vehicles: a case study for gymnasium building. Energy Build. 270, 112255 (2022). https://doi.org/10.1016/j.enbuild.2022.112255
12. Luo, Z., et al.: Joint deployment of charging stations and photovoltaic power plants for electric vehicles. Transport. Res. Transport Environ. 79, 102247 (2020). https://doi.org/10.1016/j.trd.2020.102247
13. Bhatti, A.R., Salam, Z.: A rule-based energy management scheme for uninterrupted electric vehicles charging at constant price using photovoltaic-grid system. Renew. Energy. 125, 384–400 (2018). https://doi.org/10.1016/j.renene.2018.02.126
14. Buresh, K.M., Apperley, M.D., Booysen, M.J.: Three shades of green: perspectives on at-work charging of electric vehicles using photovoltaic carports. Energy Sustain. Dev. 57, 132–140 (2020). https://doi.org/10.1016/j.esd.2020.05.007
15. Calise, F., et al.: A novel paradigm for a sustainable mobility based on electric vehicles, photovoltaic panels and electric energy storage systems: case studies for Naples and Salerno (Italy). Renew. Sustain. Energy Rev. 111, 97–114 (2019). https://doi.org/10.1016/j.rser.2019.05.022
16. Rauma, K., et al.: Overcoming non-idealities in electric vehicle charging management. IET Electr. Syst. Transp. 11(4), 310–321 (2021). https://doi.org/10.1049/els2.12025
17. Rauma, K., et al.: Network-adaptive and capacity-efficient electric vehicle charging site. IET Gener. Transm. Distrib. 16(3), 548–560 (2022). https://doi.org/10.1049/gtd2.12301
18. Simolin, T., et al.: Foundation for adaptive charging solutions: optimised use of electric vehicle charging capacity. IET Smart Grid. 4(6), 599–611 (2021). https://doi.org/10.1049/stg2.12043
19. DIgSILENT GmbH Germany.: DIgSILENT PowerFactory (2021). https://www.digsilent.de/en/
20. Python. org.: Python Release Python 3.6.6 (2018). https://www.python.org/downloads/release/python-366/
21. Spina, A., et al.: Smart grid technology Lab—A full-scale low voltage research facility at TU Dortmund university. In: 2018 AEIT International Annual Conference, pp. 1–6. IEEE (2018)
22. Contact, P.: AC Charging Controller—EM-CP-PP-ETH—2902802 (2015). https://www.phoenixcontact.com/en-il/products/ac-charging-controller-em-cp-pp-eth-2902802
23. SMA Solar Technology, AG.: Technical Information—SUNNY TRI-POWER 60 / SUNNY HIGHPOWER PEAK1 / SUNNY TRI-POWER STORAGE 60—SunSpec® Modbus® Interface (2021). https://files.sma.de/downloads/STP60_SHP75_STPS60-SunSpec-Modbus-TI-en-15.pdf
24. EGSTON Power. CSU-200 (200 kVA). https://www.egstonpower.com/wp-content/uploads/2020/04/Intro-COMPISO-SYSTEM-UNIT_Scalable-Power-Electronics-System.pdf
25. Spina, A.: Advanced Laboratory Testing of Smart Grid Applications with Power Hardware-In-The-Loop Approach. Technical University of Dortmund. Dortmund (2021). https://eldorado.tu-dortmund.de/handle/2003/40529

26. West, Electricity North.: Low Voltage Network Solutions (2019). https://www.enwl.co.uk/lvns

27. Simolin, T., et al.: Assessing the influence of the temporal resolution on the electric vehicle charging load modeling accuracy. Elec. Power Syst. Res. 208, 107913 (2022). https://doi.org/10.1016/j.epsr.2022.107913

28. Caro, L.M., et al.: State of charge influence on the harmonic distortion from electric vehicle charging. IEEE Trans. Ind. Appl. 57(3), 2077–2088 (2021). https://doi.org/10.1109/tia.2021.3057350